Transl Clin Pharmacol. 2022 Dec;30(4):201-211
https://doi.org/10.12793/tcp.2022.30.e20
pISSN 2289-0882·eISSN 2383-5427

Translational and Clinical Pharmacology TCP

Original Article

Check for updates

Predicting the systemic exposure and lung concentration of nafamostat using physiologically-based pharmacokinetic modeling

Hyeon-Cheol Jeong [1], **Yoon-Jee Chae** [2], **and Kwang-Hee Shin** [1,*]

[1]Research Institute of Pharmaceutical Sciences, College of Pharmacy, Kyungpook National University, Daegu 41566, Korea
[2]Research Institute of Pharmaceutical Sciences, College of Pharmacy, Woosuk University, Wanju 55338, Korea

OPEN ACCESS

Received: Nov 10, 2022
Revised: Dec 13, 2022
Accepted: Dec 15, 2022
Published online: Dec 21, 2022

***Correspondence to**
Kwang-Hee Shin
Research Institute of Pharmaceutical Sciences, College of Pharmacy, Kyungpook National University, 80 Daehak-ro, Buk-gu, Daegu 41566, Korea.
Email: kshin@knu.ac.kr

ORCID iDs
Hyeon-Cheol Jeong
https://orcid.org/0000-0002-3500-6694
Yoon-Jee Chae
https://orcid.org/0000-0003-4921-4192
Kwang-Hee Shin
https://orcid.org/0000-0002-0915-2700

Funding
This work was supported by the National Research Foundation of Korea (NRF) grant funded by the Korean government (MSIT) (No. NRF-2020R1C1C1013631, 2021R1A6A3A13045188) and the 4TH BK21 project (Educational Research Group for Platform Development of Management of Emerging Infectious Disease) funded by the Korean Ministry of Education (5199990614732).

ABSTRACT

Nafamostat has been actively studied for its neuroprotective activity and effect on various indications, such as coronavirus disease 2019 (COVID-19). Nafamostat has low water solubility at a specific pH and is rapidly metabolized in the blood. Therefore, it is administered only intravenously, and its distribution is not well known. The main purposes of this study are to predict and evaluate the pharmacokinetic (PK) profiles of nafamostat in a virtual healthy population under various dosing regimens. The most important parameters were assessed using a physiologically based pharmacokinetic (PBPK) approach and global sensitivity analysis with the Sobol sensitivity analysis. A PBPK model was constructed using the SimCYP® simulator. Data regarding the *in vitro* metabolism and clinical studies were extracted from the literature to assess the predicted results. The model was verified using the arithmetic mean maximum concentration (C_{max}), the area under the curve from 0 to the last time point (AUC_{0-t}), and AUC from 0 to infinity ($AUC_{0-\infty}$) ratio (predicted/observed), which were included in the 2-fold range. The simulation results suggested that the 2 dosing regimens for the treatment of COVID-19 used in the case reports could maintain the proposed effective concentration for inhibiting severe acute respiratory syndrome coronavirus 2 entry into the plasma and lung tissue. Global sensitivity analysis indicated that hematocrit, plasma half-life, and microsomal protein levels significantly influenced the systematic exposure prediction of nafamostat. Therefore, the PBPK modeling approach is valuable in predicting the PK profile and designing an appropriate dosage regimen.

Keywords: Nafamostat; COVID-19; Pharmacokinetics; SimCYP

INTRODUCTION

Nafamostat was originally developed as a synthetic serine protease inhibitor, similar to trypsin and thrombin [1]. The main indications for nafamostat are disseminated intravascular coagulation, acute pancreatitis, and anticoagulant therapy for patients undergoing continuous renal replacement [1,2]. The pharmacokinetic (PK) profile of nafamostat is not well known. However, it appears to have extensive distribution and

Conflict of Interest
- Authors: Nothing to declare
- Reviewers: Nothing to declare
- Editors: Nothing to declare

Reviewer
This article was reviewed by peer experts who are not TCP editors.

Author Contributions
Conceptualization: Jeong HC, Chae YJ, Shin KH; Data curation: Jeong HC, Chae YJ, Shin KH; Methodology: Jeong HC, Chae YJ, Shin KH; Resources: Jeong HC, Chae YJ, Shin KH; Supervision: Shin KH; Validation: Jeong HC; Writing - original draft: Jeong HC; Writing - review & editing: Jeong HC, Chae YJ, Shin KH.

elimination profiles. A previous clinical study evaluated PK profiles after IV infusion of 10, 20, and 40 mg of nafamostat for 2 hours using compartmental analysis [3]. The mean and standard deviation (SD) of area under the curve from 0 to the last time point (AUC_{0-t}) in the 3 dosage groups were 1,438.7 ± 284.84; 3,382.3 ± 1,772.5; and 6,577.3 ± 1,531.1 ng·min/mL. The maximum concentrations (C_{max}) in the 3 dosage groups were 14.49 ± 3.88, 40.4 ± 12.5, and 60.4 ± 15.8 ng/mL. As the AUC and C_{max} increase in proportion to the dose, they are considered to have linear PK profiles. Nafamostat is mainly metabolized to 6-amidino-2-naphthol and *p*-guanidinobenzoic acid by arylesterase and carboxylesterase (CES) in the blood, plasma, and various tissues, especially the liver [4,5].

Various drug repurposing studies are underway for using nafamostat for other indications. Drug repurposing refers to using approved drugs for new indications [6]. Several studies have confirmed the promising role of nafamostat in the treatment of coronavirus disease 2019 (COVID-19) and as a neuroprotective agent for degenerative brain diseases. Activation of the spike protein of severe acute respiratory syndrome coronavirus 2 (SARS-CoV-2) by transmembrane protease serine 2 (TMPRSS2) is a critical process involved in host cell fusion and bronchial infection [7,8]. Analysis of the half maximal effective concentration (EC_{50}) of camostat mesylate and nafamostat mesylate for 3 types of coronaviruses, Middle East respiratory syndrome coronavirus, SARS-CoV, and SARS-CoV-2, indicated that nafamostat has a lower EC_{50} than camostat against all coronaviruses used in the study [8]. *In vitro* assay and *in silico* prediction of molecular docking suggested that *p*-guanidinobenzoic acid is the primary active moiety that confers the pharmacological activities of nafamostat [9,10]. *p*-guanidinobenzoic acid also drives the inhibitory mechanisms of bovine trypsin and TMPRSS2 by forming a covalent complex with the enzyme. Furthermore, nafamostat exhibits neuroprotective activity by activating tyrosine receptor kinase B, extracellular signal-regulated kinase 1/2, cAMP-response element binding protein, inhibition of cyclin-dependent kinase 5, and antagonism of the N-methyl-D-aspartate receptor [1,11].

Numerous studies have been conducted on various indications using nafamostat. However, animal and clinical studies are limited, likely owing to the instability and polarity of nafamostat [12,13]. Notably, the reported half-life of nafamostat in plasma is up to 8 min, indicating that nafamostat is rapidly metabolized in the plasma. The presence of polar groups, such as guanidine, in nafamostat causes inadequate retention, interference, and analyzed results under reverse-phase bioanalytical conditions [14,15]. Consequently, insufficient *in vivo* data can be a potential barrier to the drug repurposing process while exploring the potential of repurposing and deciding on further steps.

Physiologically based pharmacokinetic (PBPK) models based on a bottom-up approach using *in vitro* absorption, distribution, and elimination data can help predict PK profiles or drug-drug interactions in drug development stage or post-market study. Recently, new drug applications using PBPK modeling were submitted to regulatory agencies, such as the US Food and Drug Administration (FDA) and European Medicines Agency. From 2013–2019, the percentage of new drug applications submitted to the FDA that used PBPK modeling increased from 20–45% [16]. PBPK modeling is used for predicting PK profiles as well as for enzyme- or transporter-mediated drug-drug interactions or for predicting PK profiles for special populations such as hepatic and renal impairment and pediatric populations [17]. For instance, the PBPK model for tetrahydrocannabinol and 11-hydroxy-tetrahydrocannabinol that developed and validated with observations of healthy and non-pregnant populations was applied to predict systemic exposure to during pregnancy [18]. The PBPK model was used

https://doi.org/10.12793/tcp.2022.30.e20

to evaluate the effect of renal function on the PK profile when rivaroxaban and amiodarone were co-administered to the elderly population [19]. Additionally, the authors quantified the impact of age and renal organic anion transporter 3 on the fold-change of the AUC of rivaroxaban using sensitivity analysis.

Sensitivity analysis is valuable for recognizing parameters that significantly influence the model prediction results. The commonly used local sensitivity analysis can analyze the effect of parameters on the model prediction results; however, it cannot evaluate the interaction among input parameters because it is based on a single parameter [20]. A global sensitivity analysis is able to simultaneously analyze the interactions between various parameters to overcome this limitation [20]. The Sobol sensitivity analysis, a general global sensitivity analysis method, does not depend on the assumption between the input and output of the model and can evaluate the interaction between parameters; however, it requires high computing power [20].

The purposes of this study were to (1) construct a nafamostat PBPK model, (2) evaluate the reported dosing regimen for the treatment of COVID-19, and (3) assess the importance of input parameters using global sensitivity analysis.

METHODS

PBPK model development

The nafamostat PBPK models were constructed using the SimCYP® simulator version 21 (Certara, Princeton, NJ, USA). The observed plasma nafamostat concentration profiles were extracted from the literature using an Engauge digitizer to verify and improve the model. All the input parameters for the nafamostat are presented in **Table 1**. Input parameters, such as microsomal CES2 clearance (CL), tissue:plasma partition coefficient (Kp) scalar, and renal CL, were obtained from previous studies or parameter estimation. The full PBPK model and Rodger and Rowland method (method 2) were applied to the distribution module to consider the tissue distribution profiles. An enzyme kinetics module was applied as an elimination model to consider plasma esterase half-life and CES2 CL. The reported plasma esterase half-life ranges from 8–41.9 minutes [5,21]. As the excretion rate of the unchanged form in urine was unclear, it was estimated using clinical research data. Additional systemic CL was estimated to consider the elimination pathway other than the established esterase-mediated metabolism.

Model simulation and verification

In the model development and evaluation process, the study design, including the dosing regimen, was set similar to that used in clinical studies [3,22]. The clinical study included healthy Chinese individuals aged 20–30 years; however, the sex ratio was not defined. Therefore, the simulation conditions in the current study were set as follows: the age of the virtual volunteers and the sex ratio were set to 20–40 years and 50:50, respectively. The dosing regimen was set as an intravenous (IV) infusion of 10, 20, and 40 mg nafamostat for 2 hours to verify the developed model. In the simulation, total 1,000 virtual volunteers (100 subjects × 10 trials) were participated. The predicted and observed PK parameters were compared to evaluate the model prediction results. The predicted/observed ratios for C_{max}, AUC_{0-t}, and AUC from 0 to infinity ($AUC_{0-\infty}$) were calculated to estimate the prediction power.

https://doi.org/10.12793/tcp.2022.30.e20

Table 1. Input parameters for the final nafamostat model

Parameters	Value	Source
Phys-chem properties		
Molecular weight (g/mol)	347.378	Drugbank
LogP	2.52	Drugbank
Compound type	Monoprotic base	
pKa	11.32	Predicted using ChemAxon
B/P	1.19	Predicted in SimCYP®
f_u	0.46	Predicted in SimCYP®
Distribution		
Distribution model	Full PBPK	
Kp scalar	2.18	Parameter estimation
V_{ss} (L/kg)	11.66	Adjusted by Kp scalar
Prediction model	Method 2 (Rodgers & Rowland model)	
Elimination		
CL type	Enzyme kinetics	
CES2 V_{max} (pmol/min/mg protein)	26,900	[5]
CES2 K_m (μM)	1,790	[5]
Plasma esterase half-life (min)	0.63	Parameter estimation
Additional HLM CL_{int} (μL/min/mg protein)	16.96	[27]
Additional HLC CL_{int} (μL/min/mg protein)	73	[27]
CL_R (L/h)	0.56	Parameter estimation
Additional systemic CL (L/h)	0.02	Parameter estimation

B/P, blood-to-plasma partition coefficient; f_u, unbound fraction; K_m, Michaelis constant; V_{max}, maximum rate in the reaction; V_{ss}, volume of distribution at steady state; CL_{int}, intrinsic clearance; CL_R, renal clearance; HLM, human liver microsome; HLC, human liver cytosol; CES, carboxylesterase.

Model application: assessment of dosing regimen for treating COVID-19

The concentrations of nafamostat in plasma and lung tissue were simulated after IV infusion of 200 mg and 4.8 mg/kg nafamostat for 24 hours [23,24] to confirm clinical case reports of *in vitro* half maximal inhibitory concentration (IC_{50}) values (approximately 10 nM) and therapeutic concentrations reported in the literature (30–240 nM) [23,24]. The dosing regimen for COVID-19 treatment was obtained from phase 1 and 2 clinical trials for approval of nafamostat as a novel drug for COVID-19 treatment or case reports describing clinical changes that occurred after nafamostat was administered to COVID-19 patients [23,24].

Global sensitivity analysis

Global sensitivity analysis was performed on 22 parameters that reportedly affect the prediction results during the model improvement involved in the distribution and elimination process to quantitatively evaluate the effect of physiological or drug-specific parameters on the prediction power. The influence of the parameters on the PK profiles of nafamostat was evaluated using 2 sensitivity indices. The first-order index evaluates the influence of individual parameters on the model, and the total-order index contains both the impact of individual parameters and the correlation with other parameters. The closer is sensitivity index to 0, the less effect it has on the model. Increasing proximity to a value of 1 enhances its impact on the model. In this study, the parameters with 2 indices exceeded 0.05 and hence were regarded as significantly affecting the robustness of the developed model [20].

RESULTS

Model verification

The constructed model was validated using the observed nafamostat concentration-time and PK profiles. For IV infusion of 10, 20, and 40 mg nafamostat for 2 hours, most

https://doi.org/10.12793/tcp.2022.30.e20

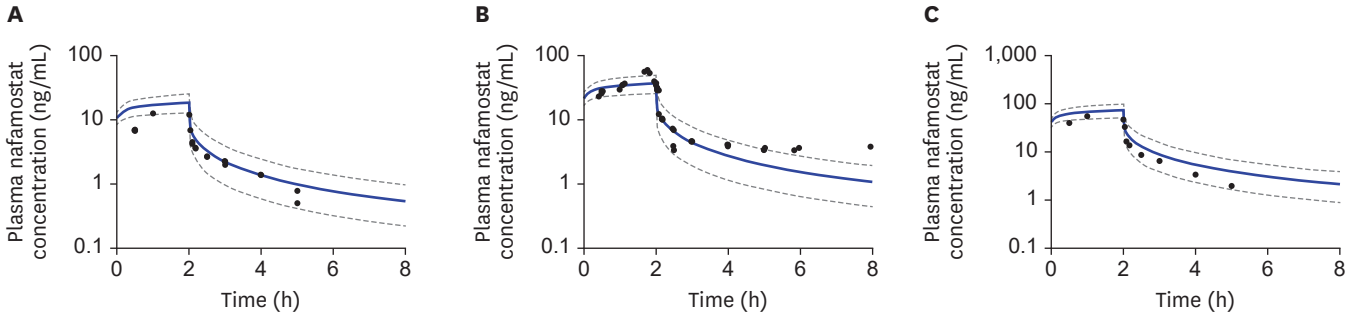

Figure 1. The observed black circle and predicted (n = 1,000, blue solid line) time-plasma concentration profiles after single intravenous infusion of (A) 10 mg, (B) 20 mg, and (C) 40 mg nafamostat. The grey dotted line represents the 5th and 95th percentile.

Table 2. Observed and predicted $AUC_{0\text{-last}}$, $AUC_{0\text{-}\infty}$, C_{max} arithmetic means and their ratios for nafamostat

Parameters	Observed [22] (n = 10)	Predicted (n = 1,000)	Mean ratio ± SD_{ratio} (range)
10 mg administration			
$AUC_{0\text{-last}}$ (ng·h/mL)	24.00 ± 4.75	41.70 ± 9.11 (27.50–57.60)	1.74 ± 0.51 (1.23–2.25)
$AUC_{0\text{-}\infty}$ (ng·h/mL)	27.60 ± 4.59	45.30 ± 10.50 (28.90–63.20)	1.64 ± 0.47 (1.17–2.11)
C_{max} (ng/mL)	14.50 ± 3.88	18.50 ± 3.61 (12.80–24.80)	1.28 ± 0.42 (0.85–1.70)
20 mg administration			
$AUC_{0\text{-last}}$ (ng·h/mL)	56.40 ± 28.70	83.50 ± 18.20 (55.10–115.10)	1.48 ± 0.82 (0.66–2.30)
$AUC_{0\text{-}\infty}$ (ng·h/mL)	59.50 ± 21.50	90.60 ± 21.10 (57.80–126.40)	1.52 ± 0.65 (0.87–2.18)
C_{max} (ng/mL)	40.40 ± 12.50	36.90 ± 7.21 (25.50–49.60)	0.91 ± 0.33 (0.58–1.25)
40 mg administration			
$AUC_{0\text{-last}}$ (ng·h/mL)	110.00 ± 25.50	167.00 ± 36.50 (110.10–230.30)	1.52 ± 0.48 (1.03–2.00)
$AUC_{0\text{-}\infty}$ (ng·h/mL)	115.00 ± 26.10	181.00 ± 42.10 (115.60–252.70)	1.57 ± 0.51 (1.06–2.09)
C_{max} (ng/mL)	60.40 ± 15.80	73.90 ± 14.40 (51.00–99.30)	1.22 ± 0.40 (0.82–1.62)

Observed PK parameters are presented as mean ± SD, and predicted PK parameters are presented as mean ± SD (5th–95th percentile). The mean ratio was calculated as $\frac{Predicted}{Observed}$.
SD, standard deviation; PK, pharmacokinetic; $AUC_{0\text{-last}}$, area under the curve time 0 to last sample point; $AUC_{0\text{-}\infty}$, area under the curve time 0 to infinity; C_{max}, maximum concentration.

of the observed plasma nafamostat concentration profiles were fitted to the predicted mean concentration and the 5th and 95th percentile ranges of the predicted mean plasma concentration-time profiles (**Fig. 1**). The predicted arithmetic mean ratios of $AUC_{0\text{-t}}$, $AUC_{0\text{-}\infty}$, and C_{max} were 1.74, 1.64, 1.28 for 10 mg, 1.48, 1.52, 0.91 for 20 mg, and 1.52, 1.57, and 1.22 for 40 mg, respectively (**Table 2**).

Model application: assessment of dosing regimen for COVID-19 treatment

After applying the dosing regimen used for COVID-19 treatment [1) 200 mg/24 h continuous infusion for 13 days and 2) 4.8 mg/kg/24 h continuous infusion for 13 days], the total (bound + unbound form) and unbound plasma nafamostat concentrations and the total concentration in lung tissue were predicted. The 2 dosing regimens used for COVID-19 treatment were sufficient to maintain the proposed effective concentration range (30–240 nM) for total plasma concentration, unbound plasma concentration (**Fig. 2A, B, D, and E**). Predicted nafamostat concentration in the lung tissue was maintained the *in vitro* IC_{50} (approximately 10 nM) (**Fig. 2C and F**).

Global sensitivity analysis

The parameters that had the greatest impact on AUC and C_{max} were plasma esterase half-life, plasma fold scalar, and hematocrit (**Fig. 3A and B**). Plasma fold scalar is used to predict plasma volume, and an increase in plasma fold scalar has caused a decrease in AUC and C_{max}. AUC and C_{max} were proportional to hematocrit and plasma esterase half-life. The parameters that had the greatest influence on CL were baseline level of microsomal protein, cardiac

https://doi.org/10.12793/tcp.2022.30.e20

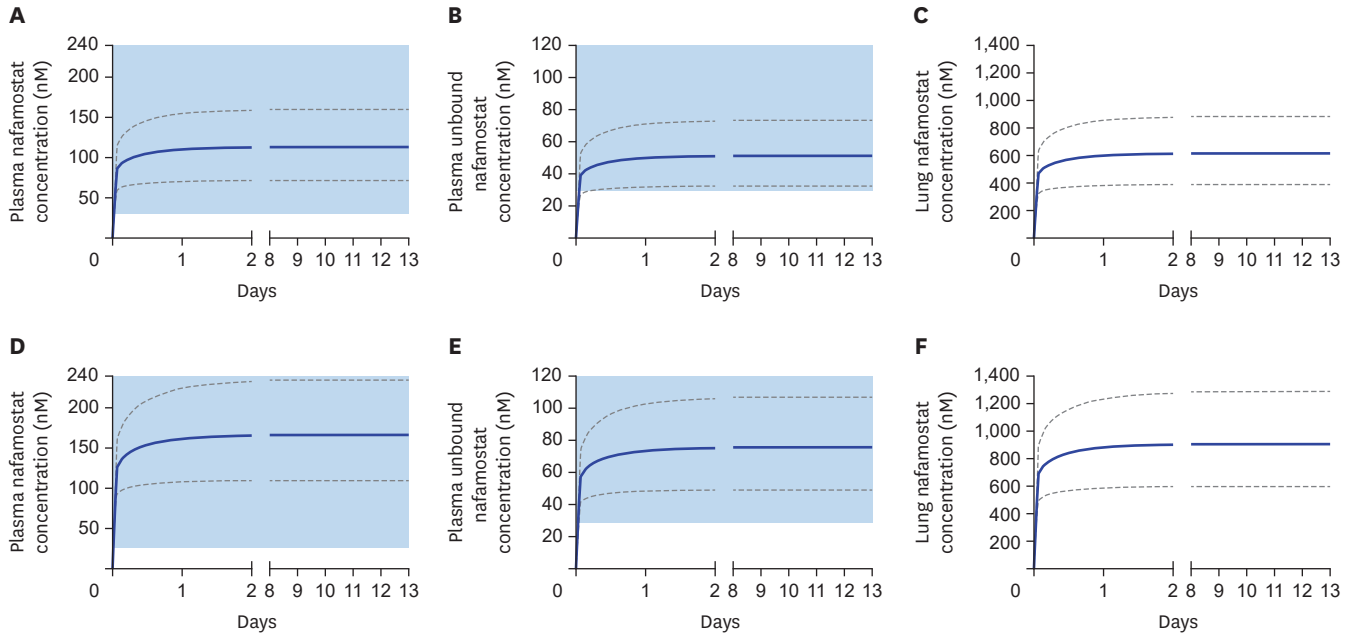

Figure 2. The predicted time-plasma and lung concentration profiles after intravenous infusion of (A-C) 200 mg/24 h and (D-F) 4.8 mg/kg/24 h nafamostat for 13 days. The grey dotted line represents 5th and 95th percentile, and blue area represents proposed therapeutic range (30–240 nM).

output scalar, and blood-to-plasma partition coefficient (B/P; **Fig. 3C**). The microsomal protein level is associated with hepatic metabolism of nafamostat, and cardiac output scalar and B/P are associated with tissue distribution. The results of global sensitivity analysis suggested that hepatic distribution and metabolism have a significant impact on systemic exposure and CL of nafamostat.

DISCUSSION

In this study, nafamostat PBPK model was successfully constructed using reported clinical, physicochemical, and metabolic data. The reported *in vitro* metabolism profiles and clinical studies data were extracted from the literature to develop and verify the model. The assessment of predicted vs. observed C_{max}, AUC_{0-t}, and $AUC_{0-\infty}$ ratios was performed, and, as a result, all the calculated PK parameter ratios were within the 2-fold range. The arithmetic means ratios of predicted vs. observed C_{max} ± SD (range) values after iv infusions of 10, 20, and 40 mg of nafamostat during 2 hours were 1.28 ± 0.42 (0.85–1.70), 0.91 ± 0.33 (0.58–1.25), and 1.22 ± 0.40 (0.82–1.62), respectively. Although the predicted plasma concentration-time profiles were well-fitted to the observations, the AUC was slightly overestimated. This problem could be affected by the high variation in observed AUC values and the variability of inter-individual or drug-specific parameters, such as intrinsic CL for esterase or half-life for plasma esterase. The percentages of the coefficient of variance for the calculated observed AUC_{0-t} and $AUC_{0-\infty}$ were 58.8% and 50.0%, respectively [3]. The minimum–maximum values for individual AUC_{0-t} and $AUC_{0-\infty}$ were 20–105.28 ng·h/mL and 31.05–117.73 ng·h/mL, respectively. This phenomenon is likely attributed to the highly unstable and polar properties of nafamostat, thereby affecting the results of the PK study. The constructed PBPK model was applied to predict the PK profiles for the reported COVID-19-treatment dosing regimens.

https://doi.org/10.12793/tcp.2022.30.e20

PBPK modeling is valuable for clinical study design and optimal dose design for drug repurposing. Rajoli et al. [25] developed a whole-body PBPK model for nitazoxanide, an anthelmintic drug, and used an *in vitro* half maximal effective concentration for SARS-CoV-2 to design an optimal dosage regimen for COVID-19 treatment. In a study by Idkaidek et al. [26], the PBPK model for hydroxychloroquine was utilized to design the dose for the inhalation formulation required to maintain an effective concentration in the alveolus. The

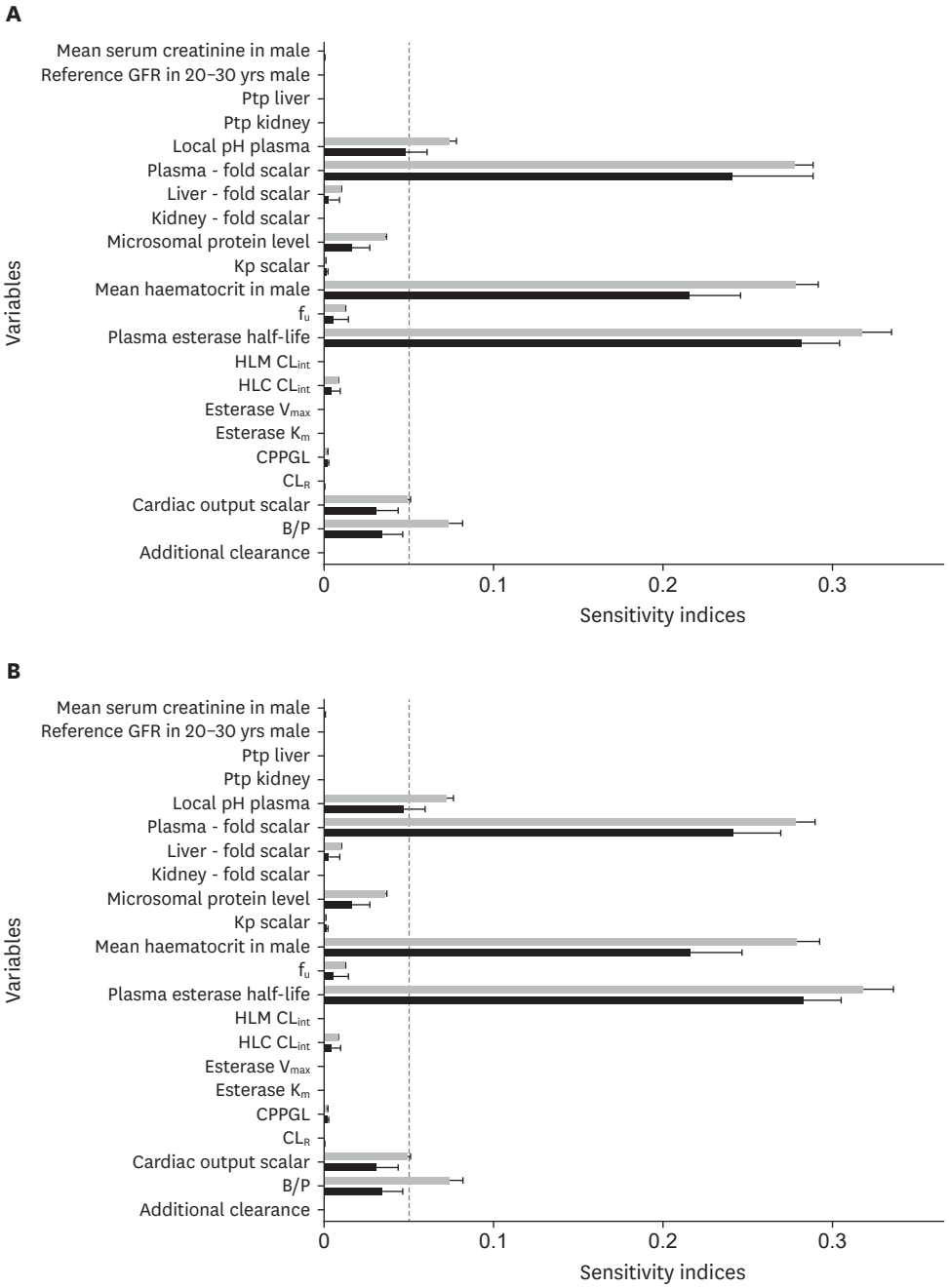

Figure 3. The first order (black bar) and total order (grey bar) sensitivity indices for (A) area under the curve, (B) maximum concentration, and (C) systemic clearance. The error bar denotes the standard deviation.
Ptp, partition coefficient of tissue:plasma; f_u, unbound fraction; HLM, human liver microsome; HLC, human liver cytosol; V_{max}, maximum velocity of an enzymatic reaction; K_m, Michaelis constant; CL_{int}, intrinsic clearance; CL_R, renal clearance; B/P, blood-to-plasma partition coefficient; GFR, glomerular filtration rate; CPPGL, cytosolic protein per gram of liver.

(continued to the next page)

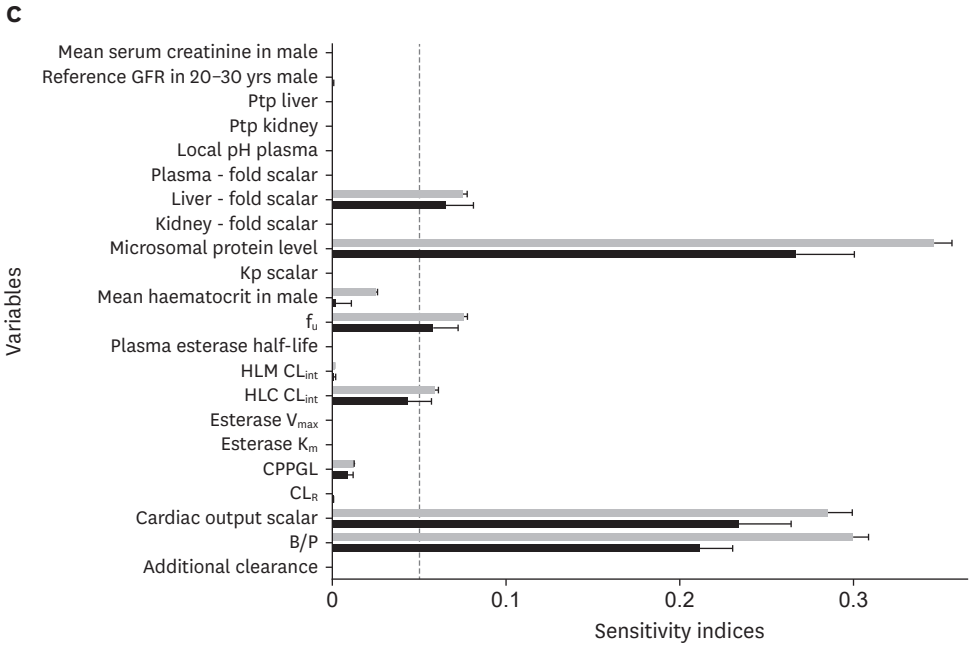

Figure 3. (Continued) The first order (black bar) and total order (grey bar) sensitivity indices for (A) area under the curve, (B) maximum concentration, and (C) systemic clearance. The error bar denotes the standard deviation.
Ptp, partition coefficient of tissue:plasma; f_u, unbound fraction; HLM, human liver microsome; HLC, human liver cytosol; V_{max}, maximum velocity of an enzymatic reaction; K_m, Michaelis constant; CL_{int}, intrinsic clearance; CL_R, renal clearance; B/P, blood-to-plasma partition coefficient; GFR, glomerular filtration rate; CPPGL, cytosolic protein per gram of liver.

PBPK model built using *in vitro* absorption data and a mathematical function can be used to predict the first-in-human PK profile, the PK profile in a particular population, and assess the effect of formulation changes. Evaluating the reported nafamostat dose regimen used to treat COVID-19 confirmed that the total plasma concentration, unbound concentration, and lung nafamostat concentration maintained the expected therapeutic concentration range (30–240 nM) and IC_{50} (up to 10 nM). These predictions suggest that the reported nafamostat dosing regimen for treating COVID-19 can sufficiently block viral entry; however, as it was based on *in vitro* studies, additional clinical studies are required to evaluate the *in vivo* antiviral effects.

Global sensitivity analysis results have both implications and limitations to interpret the PK characteristics of nafamostat. Nafamostat has been reported to be metabolized by erythrocytes, plasma, liver microsomal/cytosolic enzymes, esterase which is distributed in tissues, and it is reported that it can be widely distributed in tissues [3,5,27]. Therefore, global sensitivity analysis on physiological or drug-specific parameters that can affect distribution and metabolism of nafamostat has been performed. The baseline level of microsomal protein, cardiac output scalar, B/P, unbound fraction in plasma (f_u), human liver cytosol CL_{int}, and liver fold scalar showed a proportional relationship with CL. The baseline level of microsomal protein and liver fold scalar influenced CL by changes in the abundance of drug metabolism enzyme or liver volume. The perfusion rate limited distribution model, which determines the tissue distribution by the blood flow, was applied to the developed model. The changes in cardiac output scalar caused changes in blood flow to each tissue, affecting CL. B/P and f_u were screened as parameters that significantly influence CL because they affect tissue distribution, especially into the liver. Plasma esterase half-life, plasma fold scalar, and hematocrit can affect both tissue distribution and metabolism of nafamostat, however, these parameters caused an increase or decrease in AUC and C_{max} without affecting CL in the current model. This phenomenon was thought to be

https://doi.org/10.12793/tcp.2022.30.e20

caused by the metabolism of nafamostat by erythrocyte does not take into account in the current model. The enzyme kinetic or metabolism profiles for the erythrocyte of nafamostat have not been applied to the current model since this information was unclear. The other cause is half-life of the plasma esterase is not considered for CL calculation method of SimCYP®. In SimCYP® simulators, total plasma CL was calculated as the sum of liver and kidney, metabolic kidney, and additional plasma CL, and thus the effect of plasma esterase was not properly reflected in CL. Therefore, plasma volume or half-life of plasma esterase does not appear to have affected the predicted CL. Based on the results of global sensitivity analysis and reported literatures [3,5,27], the disposition process by the liver thought to have a significant effect on the metabolism of nafamostat, although the effects of erythrocyte and half-life of plasma esterase on the metabolism of nafamostat were underestimated.

Developed PBPK model with appropriate predictive power for nafamostat was developed, this study still has several limitations. The predicted-to-observed ratios of the AUC and the plasma nafamostat concentration were slightly overpredicted. Overprediction of the PK profiles of nafamostat might be attributed to insufficient disposition profiles, high inter-individual variability and also effect of infusion on disposition in the model development process. The estimated half-life of plasma esterase was less than the experimental value. However, the plasma nafamostat concentration in the infusion phase was overestimated. In the global sensitivity analysis, f_u in the plasma and B/P significantly affected the CL prediction. These results suggest that the distribution and elimination profiles of nafamostat may vary depending on the distribution of protein binding or plasma and whole blood, along with the intrinsic CL of drug metabolism enzymes during the disposition process of nafamostat. The published %CV of the observed AUC was estimated to be 58.8% [3]. A study suggested that the acceptance criteria of the PBPK model prediction results should be based on the %CV parameter [28]. When comparing results with %CV exceeding 30%, the acceptance criteria should be adjusted to wider than the 2-fold range, thereby preventing the high false-negative rate. Although the false-negative rate for AUC in this study could be increased by using the 2-fold limit as the acceptance criterion, it may also adequately explain the clinical study results even with conservative criteria. Another limitation is that the same dataset was used for model development and refinement. It is preferable to use a separate dataset to develop, improve, and verify the modeling approach. However, the sources are limited to obtaining sufficient observations for the above process. Last one is that developed model was verified using healthy populations, not COVID-19 patients. Information about typical physiological changes in COVID-19 patients are very limited. Thus, the PBPK model for nafamostat was developed and validated using dataset from the healthy population and predicted the systemic exposure of nafamostat in healthy population.

In conclusion, A PBPK model for nafamostat was successfully constructed and evaluated using a previously reported dataset. The ratios of the clinical study results and the predicted PK parameters were within a 2-fold range. When predicting the dose regimen for the treatment of COVID-19 used in the clinical study, the concentrations of nafamostat in plasma and lung tissue met the *in vitro* proposed effective concentration and IC_{50} range. In conclusion, the nafamostat PBPK model established in current study may help predict systemic exposure or lung concentration. The input parameters of the hematocrit, plasma half-life, and microsomal protein levels have the most significant influence on the model. We believe the model will help evaluate PK profiles and decision-making regarding dosing regimens in drug repurposing studies.

https://doi.org/10.12793/tcp.2022.30.e20

ACKNOWLEDGMENTS

Certara UK Limited (Simcyp Division) granted access to the Simcyp Simulators through a sponsored academic license.

REFERENCES

1. Fuwa M, Kageyama M, Ohashi K, Sasaoka M, Sato R, Tanaka M, et al. Nafamostat and sepimostat identified as novel neuroprotective agents via NR2B N-methyl-D-aspartate receptor antagonism using a rat retinal excitotoxicity model. Sci Rep 2019;9:20409.
PUBMED | CROSSREF
2. Hirota M, Shimosegawa T, Kitamura K, Takeda K, Takeyama Y, Mayumi T, et al. Continuous regional arterial infusion versus intravenous administration of the protease inhibitor nafamostat mesilate for predicted severe acute pancreatitis: a multicenter, randomized, open-label, phase 2 trial. J Gastroenterol 2020;55:342-352.
PUBMED | CROSSREF
3. Cao YG, Chen YC, Hao K, Zhang M, Liu XQ. An *in vivo* approach for globally estimating the drug flow between blood and tissue for nafamostat mesilate: the main hydrolysis site determination in human. Biol Pharm Bull 2008;31:1985-1989.
PUBMED | CROSSREF
4. Aoyama T, Okutome T, Nakayama T, Yaegashi T, Matsui R, Nunomura S, et al. Synthesis and structure-activity study of protease inhibitors. IV. Amidinonaphthols and related acyl derivatives. Chem Pharm Bull (Tokyo) 1985;33:1458-1471.
PUBMED | CROSSREF
5. Yamaori S, Fujiyama N, Kushihara M, Funahashi T, Kimura T, Yamamoto I, et al. Involvement of human blood arylesterases and liver microsomal carboxylesterases in nafamostat hydrolysis. Drug Metab Pharmacokinet 2006;21:147-155.
PUBMED | CROSSREF
6. Jourdan JP, Bureau R, Rochais C, Dallemagne P. Drug repositioning: a brief overview. J Pharm Pharmacol 2020;72:1145-1151.
PUBMED | CROSSREF
7. Fraser BJ, Beldar S, Seitova A, Hutchinson A, Mannar D, Li Y, et al. Structure and activity of human TMPRSS2 protease implicated in SARS-CoV-2 activation. Nat Chem Biol 2022;18:963-971.
PUBMED | CROSSREF
8. Hoffmann M, Schroeder S, Kleine-Weber H, Müller MA, Drosten C, Pöhlmann S. Nafamostat mesylate blocks activation of SARS-CoV-2: new treatment option for COVID-19. Antimicrob Agents Chemother 2020;64:e00754-20.
PUBMED | CROSSREF
9. Ramjee MK, Henderson IM, McLoughlin SB, Padova A. The kinetic and structural characterization of the reaction of nafamostat with bovine pancreatic trypsin. Thromb Res 2000;98:559-569.
PUBMED | CROSSREF
10. Hempel T, Raich L, Olsson S, Azouz NP, Klingler AM, Hoffmann M, et al. Molecular mechanism of inhibiting the SARS-CoV-2 cell entry facilitator TMPRSS2 with camostat and nafamostat. Chem Sci 2020;12:983-992.
PUBMED | CROSSREF
11. Liu Y, Li C, Wang J, Fang Y, Sun H, Tao X, et al. Nafamostat mesilate improves neurological outcome and axonal regeneration after stroke in rats. Mol Neurobiol 2017;54:4217-4231.
PUBMED | CROSSREF
12. Kim HA, Kim JE. Development of nafamostat mesylate immediate-release tablet by drug repositioning using quality-by-design approach. Pharmaceutics 2022;14:1219.
PUBMED | CROSSREF
13. Oh HS, Kim T, Gu DH, Lee TS, Kim TH, Shin S, et al. Pharmacokinetics of nafamostat, a potent serine protease inhibitor, by a novel LC-MS/MS analysis. Molecules 2022;27:1881.
PUBMED | CROSSREF
14. Deng P, Chen X, Zhong D. Quantification of polar drugs in human plasma with liquid chromatography-tandem mass spectrometry. Bioanalysis 2009;1:187-203.
PUBMED | CROSSREF

15. Chambers E, Wagrowski-Diehl DM, Lu Z, Mazzeo JR. Systematic and comprehensive strategy for reducing matrix effects in LC/MS/MS analyses. J Chromatogr B Analyt Technol Biomed Life Sci 2007;852:22-34.
PUBMED | CROSSREF

16. Zhang X, Yang Y, Grimstein M, Fan J, Grillo JA, Huang SM, et al. Application of PBPK modeling and simulation for regulatory decision making and its impact on US prescribing information: an update on the 2018-2019 submissions to the US FDA's office of clinical pharmacology. J Clin Pharmacol 2020;60 Suppl 1:S160-S178.
PUBMED | CROSSREF

17. Lin W, Chen Y, Unadkat JD, Zhang X, Wu D, Heimbach T. Applications, challenges, and outlook for PBPK modeling and simulation: a regulatory, industrial and academic perspective. Pharm Res 2022;39:1701-1731.
PUBMED | CROSSREF

18. Patilea-Vrana GI, Unadkat JD. Development and verification of a linked Δ^9-THC/11-OH-THC physiologically based pharmacokinetic model in healthy, nonpregnant population and extrapolation to pregnant women. Drug Metab Dispos 2021;49:509-520.
PUBMED | CROSSREF

19. Wang Z, Cheong EJ, Kojodjojo P, Chan EC. Model-based risk prediction of rivaroxaban with amiodarone for moderate renal impaired elderly population. Cardiovasc Drugs Ther. 2021 [In Press].
PUBMED | CROSSREF

20. Zhang XY, Trame MN, Lesko LJ, Schmidt S. Sobol sensitivity analysis: a tool to guide the development and evaluation of systems pharmacology models. CPT Pharmacometrics Syst Pharmacol 2015;4:69-79.
PUBMED | CROSSREF

21. Choi JY, Kang YJ, Jang HM, Jung HY, Cho JH, Park SH, et al. Nafamostat mesilate as an anticoagulant during continuous renal replacement therapy in patients with high bleeding risk: a randomized clinical trial. Medicine (Baltimore) 2015;94:e2392.
PUBMED | CROSSREF

22. Cao YG, Zhang M, Yu D, Shao JP, Chen YC, Liu XQ. A method for quantifying the unstable and highly polar drug nafamostat mesilate in human plasma with optimized solid-phase extraction and ESI-MS detection: more accurate evaluation for pharmacokinetic study. Anal Bioanal Chem 2008;391:1063-1071.
PUBMED | CROSSREF

23. Jang S, Rhee JY. Three cases of treatment with nafamostat in elderly patients with COVID-19 pneumonia who need oxygen therapy. Int J Infect Dis 2020;96:500-502.
PUBMED | CROSSREF

24. Doi K, Ikeda M, Hayase N, Moriya K, Morimura N; COVID-UTH Study Group. Nafamostat mesylate treatment in combination with favipiravir for patients critically ill with COVID-19: a case series. Crit Care 2020;24:392.
PUBMED | CROSSREF

25. Rajoli RK, Pertinez H, Arshad U, Box H, Tatham L, Curley P, et al. Dose prediction for repurposing nitazoxanide in SARS-CoV-2 treatment or chemoprophylaxis. Br J Clin Pharmacol 2021;87:2078-2088.
PUBMED | CROSSREF

26. Idkaidek N, Hawari F, Dodin Y, Obeidat N. Development of a physiologically-based pharmacokinetic (PBPK) model of nebulized hydroxychloroquine for pulmonary delivery to COVID-19 patients. Drug Res (Stuttg) 2021;71:250-256.
PUBMED | CROSSREF

27. Yamaori S, Ukena E, Fujiyama N, Funahashi T, Kimura T, Yamamoto I, et al. Nafamostat is hydrolysed by human liver cytosolic long-chain acyl-CoA hydrolase. Xenobiotica 2007;37:260-270.
PUBMED | CROSSREF

28. Abduljalil K, Cain T, Humphries H, Rostami-Hodjegan A. Deciding on success criteria for predictability of pharmacokinetic parameters from *in vitro* studies: an analysis based on *in vivo* observations. Drug Metab Dispos 2014;42:1478-1484.
PUBMED | CROSSREF